MDPI

Article

Researching on the Deterministic Channel Models for Urban Microcells Considering Diffraction Effects

Chunzhi Hou [1], Zhensen Wu [1], Jiaji Wu [2], Yunhua Cao [1,*], Leke Lin [3], Xiangming Guo [3] and Changsheng Lu [3]

1 School of Physics and Optoelectronic Engineering, Xidian University, Xi'an 710071, China; czhou_1@stu.xidian.edu.cn (C.H.); wuzhs@mail.xidian.edu.cn (Z.W.)
2 School of Electronic Engineering, Xidian University, Xi'an 710071, China; wujj@mail.xidian.edu.cn
3 National Key Laboratory of Electromagnetic Environment, China Research Institute of Radiowave Propagation, Qingdao 266107, China; linlk@crirp.ac.cn (L.L.); guoxm@crirp.ac.cn (X.G.); lucs@crirp.ac.cn (C.L.)
* Correspondence: yhcao@mail.xidian.edu.cn

Abstract: Deterministic channel models, such as the three-dimensional (3D) ray launching method, can yield wireless channel parameters. In the non-line-of-sight (NLOS) propagation, the outdoor 3D ray launching method that considers diffraction effects is more accurate than the one that does not. While considering the diffraction effect, obtaining the diffraction point is challenging. This paper proposed a method for determining diffracted rays using the receiving sphere method in 3D ray launching. The diffraction point is determined using the shortest distance method between two straight lines, and the signal loss from the transmitting to receiving antennas is obtained. Furthermore, experiments on a millimeter wave in a microcell scenario were performed. The test results of the wireless channel parameters were compared with theoretical calculations. The results obtained via the 3D ray launching method that only considers the specular reflection and direct rays agree with the experimental results in the line-of-sight (LOS); furthermore, they generate larger errors compared with the experimental results in the NLOS. The results obtained via the 3D ray launching method that considers the direct ray, reflected rays, and diffracted rays agree with the experimental results both in the LOS and NLOS. Therefore, the 3D ray launching method that considers the diffraction effect can improve the prediction accuracy of the millimeter wave channel parameters in a microcell.

Keywords: diffraction effect; millimeter wave; deterministic channel model; three-dimensional ray launching method; microcell

1. Introduction

Compared with fifth-generation wireless systems (5G) sub-6GHz, millimeter wave technology has unique advantages, such as a large bandwidth, low delay, and high speed, and can effectively meet the needs of future wireless communication systems with respect to capacity and transmission rate [1–3]. Therefore, millimeter wave technology has become a core element of 5G.

With the rapid development of wireless mobile communication, the size of a cell is becoming smaller, and the design of a mobile system requires information on transmission at specific sites [4,5]. It is essential for a radio wave propagation model to realize a wireless system. In the past few decades, statistical and deterministic channel models have been proposed in urban microcell environments. Compared with a statistical channel model, a deterministic channel model can solve specific, real-life scenarios. Considering the future communication system design, the outdoor environment will be one of the important application scenarios in wireless communications [6], and its actual environment is complex and changeable. It is difficult for general statistical channel models to distinguish these changes, which makes it difficult to obtain an accurate model. At present, the propagation of radio waves is simulated to obtain the precise channel characteristics of a specific scene in

the deterministic channel model. Ray tracing is the main method in deterministic channel modeling and provides predictions of propagation characteristics to realize a wireless communication system [7–11].

Research and development of wireless communication systems requires an extensive understanding of the channel characteristics. Ray tracing is an effective method in wireless communication and can predict propagation characteristics very precisely. In the three-dimensional (3D) ray launching method, a large number of rays are cast from the transmitter in all directions [12–14]. The relationship between the rays and obstacles is evaluated, the path of the ray is searched, the propagation loss is calculated, and the arrival and departure angles of the receiver at a certain position are determined. For specular reflection, the path of the reflection can be obtained through the image method and the test of the intersection.

In the past few decades, a large number of measurements were conducted, and large amounts of experimental data were obtained; however, calculations and predictions have not been reported. Horikoshi et al. conducted an indoor propagation measurement at 1.2 GHz [15]. Subsequently, Bultitude et al. conducted an indoor propagation measurement [16]. Moreover, measurements at 910 MHz were compared with those at 1.75 GHz. Measurements and analyses were conducted by H. W. Arnold R. Murray et al. at 815 MHz [17]. Subsequently, Honcharenko first proposed the two-dimensional (2D) ray launching method to calculate the reflected and transmitted rays and compared the results with experimental data in 1992 [18]. The method was highly effective for complex environments. Ji Zhong et al. proposed the receiving circles to determine the occurrence of diffracted rays in a two-dimensional scenario [19]. However, there are few references on determining the three-dimensional diffraction path. Schaubach et al. first proposed a method for calculating the radius of a receiving sphere in the 3D ray launching method [20]. Subsequently, Hewei et al. proposed a receiving cylinder to determine whether the diffracted rays were received [21]. Geok proposed the maximum accuracy technology of the indoor 3D minimum ray launching method, which is suitable for effective indoor radio wave propagation prediction [22]. In 2019, Hossain et al. proposed an effective 3D ray launching method to study the indoor radio waves at 28 GHz [23]. Therefore, it is necessary to study methods to determine the diffraction point in case of 3D ray launching in outdoor microcells.

In the paper, the receiving sphere method is used to improve the method of determining the diffracted rays and the calculation accuracy of the 3D ray launching method. This study mainly focuses on the diffraction effect. The framework of the study is as follows: First, the channel measurement system is described. Second, the basic theory of the 3D ray launching method and the calculation method of the reflected and diffracted fields are introduced. Third, experimental methods are introduced. Fourth, the result of the 3D ray tracing is verified. Finally, a summary of this study is provided.

2. Theory of Ray Launching Method

2.1. Three-Dimensional Ray Launching Method

Channel models are divided into the following two categories: statistical models, also known as empirical models, and theoretical models, also called deterministic models.

Compared with statistical channel models, deterministic models explicitly consider the interaction between the transmitted electromagnetic wave and the surrounding environments. Deterministic models are suitable for predicting indoor microcellular and central areas of large cities by applying the electromagnetic field theory to calculate the specific environment. The most representative model is the ray-tracing model.

Ray tracing is a technology that is extensively used to predict the propagation characteristics of radio waves in mobile communications, personal communications (street microcell), and indoor microcells. Ray tracing can be used to identify all possible ray paths between the transmitting and receiving antennas in a multipath channel. Once all the possible rays have been identified, the amplitude, phase, delay, and polarization of each ray can be calculated based on the radio wave propagation theory. Accordingly, the coherent combination of all rays arriving at the receiving point can be obtained by

combining the antenna pattern and the bandwidth of the system. Hence, the ray-tracing model has tremendous advantages in terms of its prediction accuracy compared with traditional statistical models and can provide adequate information for the design of broadband wireless systems.

With the development of computer technology and algorithms to enhance accuracy, the ray-tracing algorithm has become a highly effective, accurate, and fast method for wireless channel modeling. Simple and easy to implement, it has been extensively used in propagation prediction in specific scenarios.

Ray-tracing methods mainly include the following two methods: (a) the image method and (b) the shooting and bouncing ray method. The image method can determine the effective reflection path between the transmitting and receiving points. However, the amount of calculation increases owing to many reflecting surfaces in a typical urban environment, and therefore, this method may no longer be applicable in a typical urban environment.

Therefore, the ray launching method is extensively used in propagation modeling. The underlying concept of the ray launching method is to track each ray emitted from the source position to determine whether the rays reach the receiving point. The steps involved are as follows:

1. Preparation work. There are three main parts. First, the environmental data file must be read, including all the vertex coordinates of the building and the outer normal vector of the wall. Second, various electromagnetic parameters must be initialized, such as the height of the transmitting and receiving antennas, frequency, emission power, wavelength, dielectric constant, and conductivity. Third, the influence of different number of rays on the accuracy of the electric field must be tested by subdividing the polyhedron to generate different types of rays. Furthermore, the regular icosahedron is used.
2. Direct rays must be assessed to determine whether the receiving antenna is within the line of sight (LOS) of the transmitting antenna.
3. The reflected and diffracted rays must be detected. The rays that enter the receiving ball after one reflection and diffraction must be identified.
4. The following must be detected: first-order diffraction ray and one diffraction ray followed by a reflected ray.
5. Multiple reflections for up to fifth order reflection rays must be detected.
6. Subsequent calculations. The electric field strength and synthesis of each ray based on the ray path must be calculated. Thus, the path loss is obtained at the receiving point. A brief flow diagram of the 3D ray launching method is shown in Figure 1.

A detailed flow chart of the serial algorithm of the 3D ray launching method is shown in Figure 2. The field strength on the direct ray, one order diffraction rays, multi-order reflection rays, the reflection followed by the diffraction rays and the diffraction followed by the reflection rays can be obtained in Figure 2, respectively. The path loss at the receiving point is calculated to obtain the sum of a single-ray power (SP) and the sum of the complex power (PS) [24,25]. Therefore,

$$L_{SP} = 10 \log_{10} \left| \sum_{i=1}^{n} \left(\frac{\lambda}{4\pi} \frac{E_i}{E_0} \right)^2 \right| \tag{1}$$

where E_i is the electric field of the ith ray in volts, E_0 is the initial field in volts, and λ is the wavelength in meters.

$$L_{PS} = 20 \log_{10} \left| \frac{\lambda}{4\pi} \frac{E_{total}}{E_0} \right| \tag{2}$$

where $E_{total} = \sum_{i=1}^{n} E_i$ is the total field strength in volts.
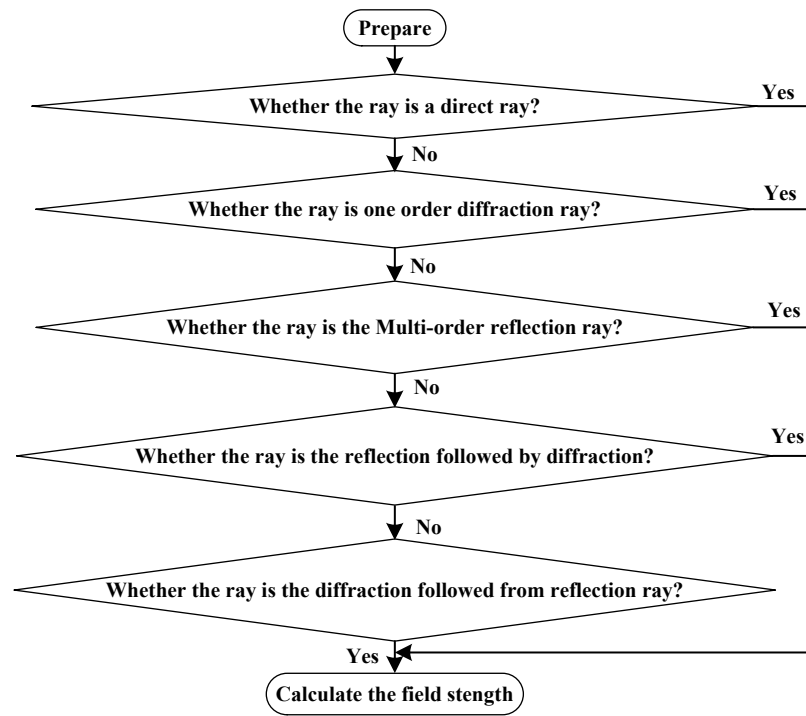
Figure 1. Flow chart of the program.
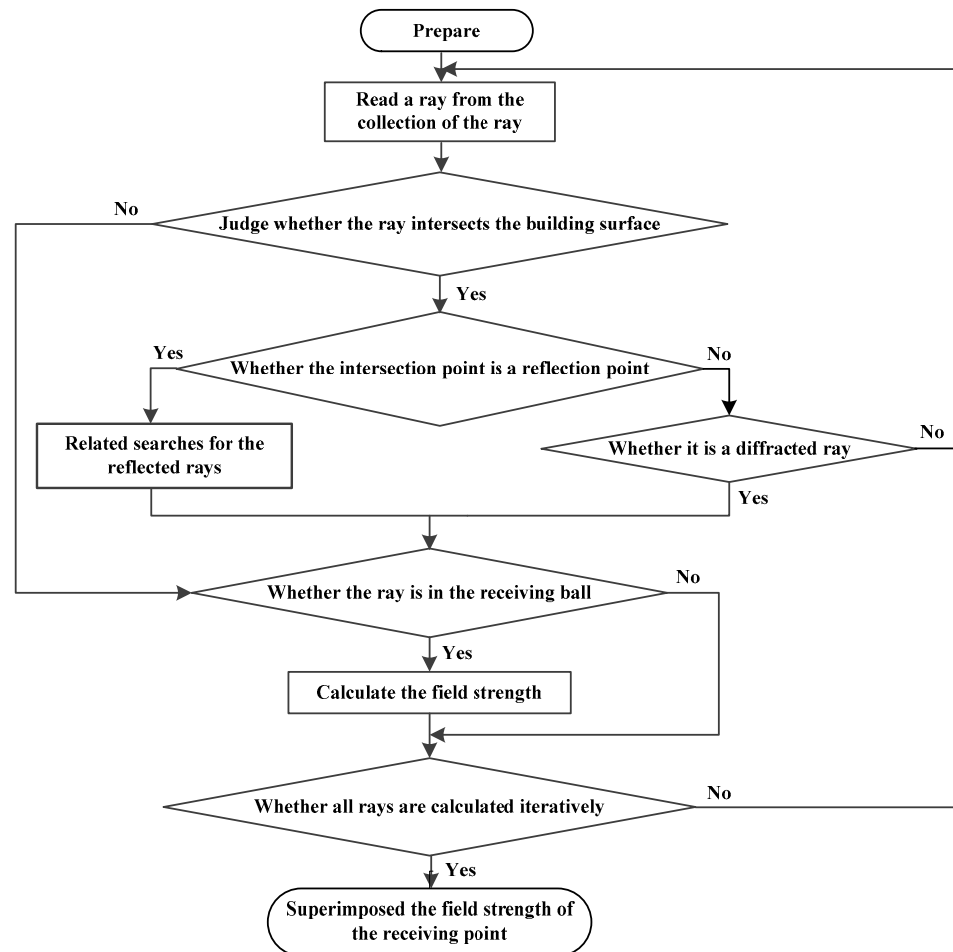
Figure 2. Detailed flow chart of the program.

2.2. Calculation of the Direct Wave Field

In the LOS, the direct wave-field strength is

$$E = E_0 \cdot e^{-jks}/s \tag{3}$$

where s is the distance between the transmitting and receiving antenna in meters, and E_0 is the initial field in volts. k is the wave number in m^{-1}.

2.3. Calculation of the Reflected Field

If the light is reflected once or multiple times before reaching the field point, the light is called a reflected ray. The ray is the reflection of electromagnetic waves at the interface of different media. The propagation direction of the reflected rays depends on the laws of reflection. The strength of the reflected field is determined by the Fresnel equation. At the boundary of the medium, the vertical polarization reflection coefficient and the parallel polarization reflection coefficient are defined as [26]

$$
\begin{aligned}
R_{//} &= \frac{\varepsilon_r \cos\theta - \sqrt{\varepsilon_r - \sin^2\theta}}{\varepsilon_r \cos\theta + \sqrt{\varepsilon_r - \sin^2\theta}} \\
R_\perp &= \frac{\cos\theta - \sqrt{\varepsilon_r - \sin^2\theta}}{\cos\theta + \sqrt{\varepsilon_r - \sin^2\theta}}
\end{aligned}
\tag{4}
$$

where θ is the incident angle in degrees, the relative permittivity is $\varepsilon_r = \varepsilon - j60\sigma\lambda$, ε is the permittivity, and σ is the conductivity.

The strength of the reflected field is [27,28]

$$E^r = E_0 \cdot R \cdot A \cdot e^{-jk(s_1+s_2)} \tag{5}$$

where E_0 is the electric field at a distance of 1 m from the transmitting antenna in volts, R is the Fresnel reflection coefficient, A is the diffusion factor from the reflection point to the field point, s_1 denotes the distance from the transmitting point to the diffraction point in meters, and s_2 denotes the distance from the diffraction point to the receiving point in meters.

2.4. Calculation of the Diffracted Field

The diffracted wave is more complicated compared with the direct and reflected waves. An incident ray will produce many diffracted rays. The calculation formula of the diffraction coefficient is as follows [29,30],

$$
D_{e,m}(\phi_2, \phi_1, \beta_0) = \frac{-e^{-j\pi/4}}{2n\sqrt{2\pi k}\sin\beta_0}
\begin{Bmatrix}
\cot\left[\frac{\pi+(\phi_2-\phi_1)}{2n}\right] F[kLa^+(\phi_2-\phi_1)] + \dots \\
\cot\left[\frac{\pi-(\phi_2-\phi_1)}{2n}\right] F[kLa^-(\phi_2-\phi_1)] + \dots \\
R_0 \cot\left[\frac{\pi+(\phi_2-\phi_1)}{2n}\right] F[kLa^+(\phi_2-\phi_1)] + \dots \\
R_h \cot\left[\frac{\pi-(\phi_2-\phi_1)}{2n}\right] F[kLa^-(\phi_2-\phi_1)]
\end{Bmatrix}
\tag{6}
$$

where e and m are the vertical and parallel polarizations, respectively. Furthermore, β_0 is the angle between the incident ray and the wedge. $F(x)$ is a transition function, which is used to correct Keller's nonuniformity correction and is a variant of the Fresnel integral. R_0 and R_n are the reflection coefficient matrices of the 'o' and 'n' planes on both sides of the diffraction edge, respectively, ϕ_1 is the angle between the incident ray and the 'o' plane in degrees, ϕ_2 is the angle formed by the diffracted rays and the 'o' plane, n is the wedge factor in degrees, and k is the number of the carrier wave in m^{-1}.

The diffraction field is [31],

$$E^d = E_0 \cdot D \cdot A \cdot e^{-jk(s_1+s_2)} \tag{7}$$

where D is the diffraction coefficient, and A is the diffusion factor.

A quick and effective method is proposed herein to determine the diffraction point. As shown in Figure 3, the intersection O_1 between any ray l and the wall is assessed. If the intersection is a virtual point, the corresponding diffraction point O on the edge of the wall will be determined based on the method of determining the shortest distance between two straight lines. Assuming that the distance between the transmitting and the diffraction point is d, the diffraction point O is the center of the circle, and the radius $\varphi d / \sqrt{3}$ is used to determine whether the ray has an intersection with the circle. If there is an intersection, the ray is diffracted; otherwise, no diffraction occurs.
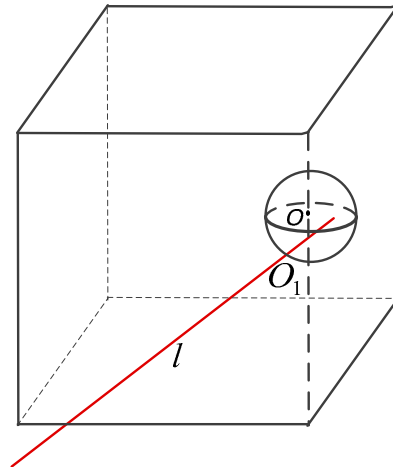
Figure 3. Schematic showing the method used to determine the diffraction point. The red line represents ray l, the cuboid denotes the barrier, the sphere represents a virtual receiving sphere, O is the center of the virtual receiving sphere, and O_1 is the point where the ray l intersects with the virtual receiver sphere.

3. Experimental Methods: Introduction to Channel Measurements at 39 GHz

3.1. Channel Measurement System at 39 GHz

The available bandwidth of the 5G millimeter-wave frequency band is as high as several gigahertz. This increased bandwidth introduces considerable challenges to the channel measurement equipment. Traditionally, the broadband channel measurement methods include direct radio frequency pulse, spread-spectrum sliding correlation, and frequency-domain sweep measurements. The method of the spread-spectrum sliding correlation measurement has become the main method of channel measurements owing to its advantages of high processing gain and coverage in the millimeter wave band.

The measurement system used is based on a spread-spectrum sliding correlation principle:

$$\gamma[m] = \sum_{n=m}^{m+L-1} y_l[n] y_l^*[n+N] \tag{8}$$

where L is denotes as the actual number of samples averaged in windows, $y_l[n]$ is the received signal in the time domain at the nth moment, and $y_l^*[n+N]$ denotes the conjugate of the received signal in the time domain at the $(n+N)$th moment. The system has the ability to measure multi-antenna broadband channels in the millimeter-wave frequency band. A rubidium atomic clock is calibrated using the global positioning system (GPS) for time synchronization.

According to the measurement requirements, the measurement points can be planned independently for the transmitter and receiver in the long-distance measurement range. The system is equipped with a 3D antenna turntable, which can accurately control the vertical, horizontal, and pitch rotation angles of the antennas. As shown in Figure 4, the transmitter terminal of the system is mainly composed of a rubidium atomic clock, an M8190 arbitrary waveform generator, E8267D vector signal source, and an analog

signal source. The rubidium atomic clock provides a reference signal for time, and M8190 generates analog measurement signals. Furthermore, baseband signals are up-converted to radio frequency signals by the E8267D signal source, and the analog signal source provides a local oscillator signal based on certain conditions.
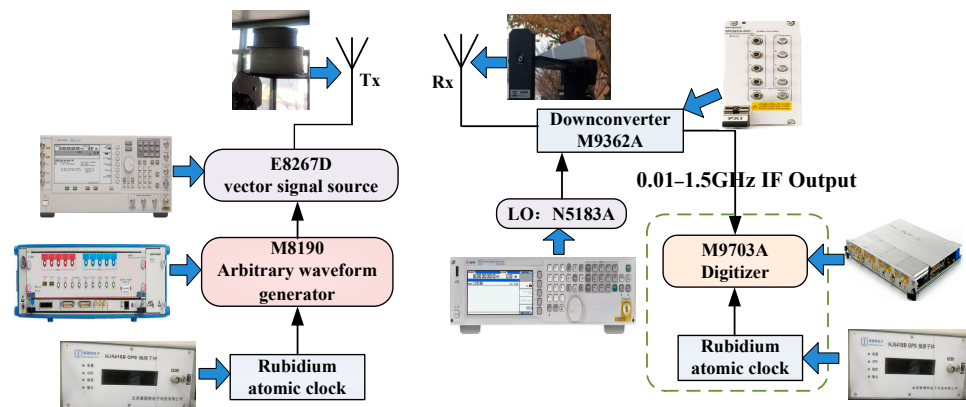
Figure 4. Measurement system used for millimeter waves.

The receiving terminal is mainly composed of a down-converter M9362A, the signal source N5183A, and the digitizer M9703A. The radio frequency input range of the down-converter M9362A is 10 MHz to 40 GHz. The N5183A provides the local oscillator signal for the down-converter. The frequency range of the intermediate frequency signal output by the N9362A is in the range of 0.01 to 1.5 GHz, and the M9703A digitizer samples the intermediate frequency signal. GPS signals are used to calibrate the rubidium atomic clocks. The system has a very high temporal synchronization accuracy and supports long-distance measurements.

The transmitting antenna is omnidirectional, and the antenna pattern of the transmitting antenna is shown in Figure 5. Moreover, the operating frequency ranges from 26.5 to 40 GHz. The gain of the omnidirectional antenna at 39 GHz is 6.19 dBi. The receiving antenna is a directional horn antenna. The operating frequency is in the range of 26.3 to 40 GHz. The gain of the horn antenna at 39 GHz is 26.92 dBi, and the half-power beamwidth of the E and H planes are 7.41° and 7.8°, respectively. The transmitting and receiving antennas are operated in vertical polarization modes.
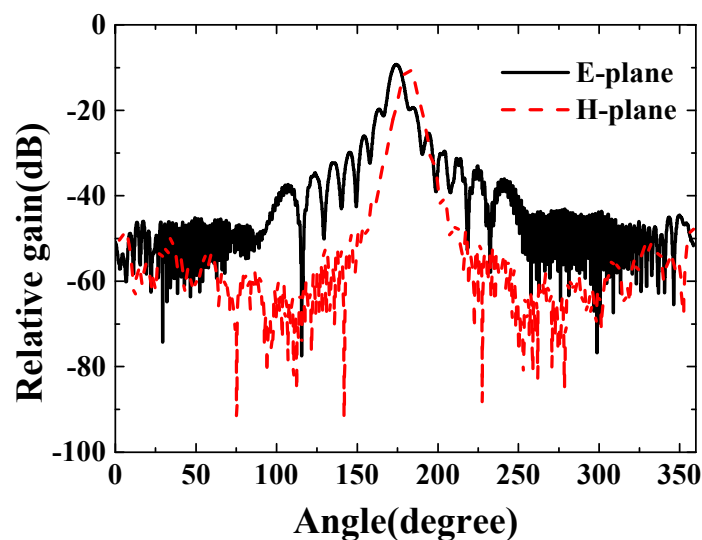
Figure 5. Horn antenna pattern at 39 GHz. (The red line is antenna pattern of H-plane, and the black line is antenna pattern of E-plane.)

3.2. Channel Measurement Procedure

In this study, measurements were conducted in urban microcells. An omnidirectional antenna, which was fixed at a position to set it in a vertically polarized state, was adopted in the transmitting terminal. The receiving terminal used a horn antenna, and a turntable was used to move in the horizontal and vertical directions, respectively. Different measurement areas were selected for LOS and NLOS measurements based on the distribution of buildings. The transmitter position was fixed during the measurement. Moreover, different measurement points were selected as receivers, including 22 points for LOS and 11 points for NLOS. The distribution of the specific measurement points is shown in Figure 6. The red solid line represents the x- and y-axes, and the z-axis is along the direction of the height of the building. The blue line represents the lawn. In the LOS scenario, the transmitting antenna is an omnidirectional antenna, and its coordinates are Tx1 (22.3, 64.9, 9). The receiving antenna is a horn antenna, and it moves along the yellow line (that is, along the x-axis) every 5 or 10 m; y = 71.3, z = 1.5, and x assumes the following values: 42.3, 47.3, 52.3, 57.3, 62.3, 67.3, 72.3, 77.3, 82.3, 87.3, 92.3, 97.3, 102.3, 107.3, 112.3, 122.3, 132.3, 142.3, 152.3, 162.3, 172.3. The power of the transmitter is 0 dBm, and the bandwidth of the measurement is 1 GHz. The azimuthal angle is collected every 5°. The transmitter antenna is in a vertically polarized state, and the receiving antenna is also in a vertically polarized state. In the NLOS scenario, the transmitting antenna is an omnidirectional antenna, and Tx2 is (2.9, 54.7, 9); the receiving antenna is a horn antenna that moves once every 5 m along the gray lines. The transmitting antenna and receiving antenna are vertically polarized.
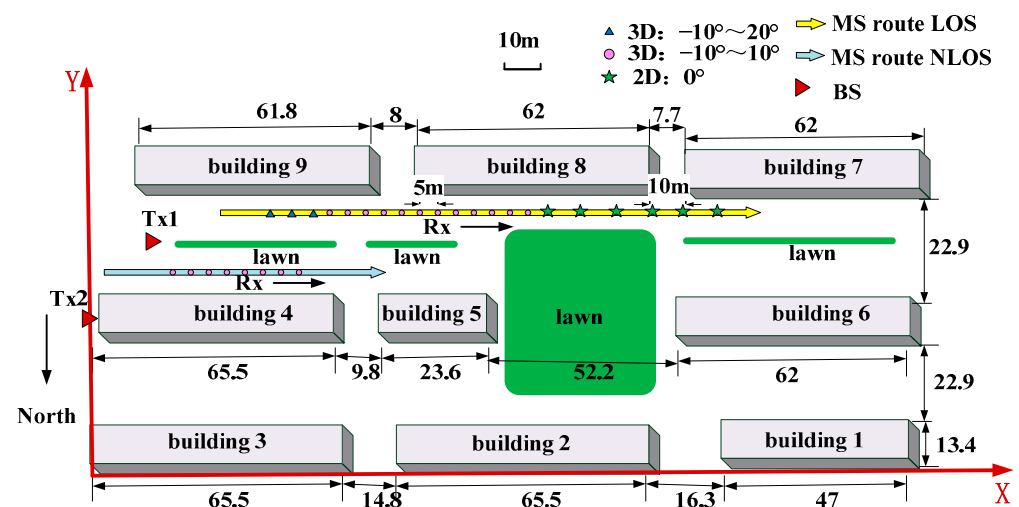
Figure 6. Plot of measurements in urban microcells.

The measurement parameters are listed in Table 1. The complex relative dielectric permittivity of the wall is taken as $\varepsilon_r = 3 + 0.005i$ based on the value provided in the literature [32]. The farther the receiving antenna is from the transmitting antenna, the smaller the influence of the elevation angle. Therefore, the station that is far away from the transmitting antenna only measured an elevation angle of 0° and azimuthal angle of 360°, as shown in Figure 6. In Figure 6, 3D indicates that the elevation and azimuthal angles are measured; 2D indicates the experimental data where the elevation angle is 0° and the azimuthal angle is 360°.

Table 1. Channel measurement parameters in the urban microcell.

Parameters	Value
Frequency (GHz)	39
Bandwidth (GHz)	1
Transmitting power (dBm)	0
The height of receiver/transmitter antenna (m)	1.5/9.0
The transmitter and the gain (dBi)	Omnidirectional antenna/6.19
The receiver and the gain (dBi)	Horn antenna/26.92
The step of the receiver antenna (°)	5°
Polarization mode of transmitting antenna	V
Polarization mode of receiving antenna	V

In LOS environments, the transmitting Tx1 was fixed, and the receiving antenna was movable. In the short range, the azimuthal angle of each receiving point was measured at $-10°$, $0°$, $10°$, $20°$, $30°$, and the elevation angle of each receiving point was measured every $5°$. For longer distances, the elevation angle of each receiving point was measured at $0°$ and the azimuthal angle of the receiving point was measured every $5°$. In the NLOS environments, the transmitting point, which is referred to as Tx2, was fixed, and the receiving antenna was moved. In the 3D measurements, the receiving point that was close to the transmitting point was measured at azimuthal angles of $-10°$, $0°$, $10°$, $20°$, and $30°$, and at every $5°$ in the case of the elevation angles. The receiving point that was far from the transmitting point was at $-10°$, $0°$, and $10°$ in terms of azimuthal angles and every $5°$ in the case of elevation angles. Finally, the data were collected and processed as shown in Figure 7.
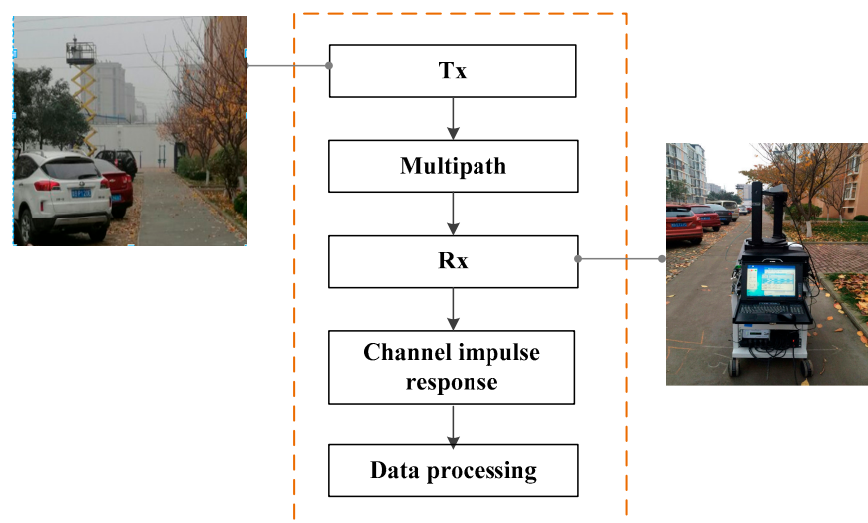
Figure 7. Flow chart outlining the data processing.

4. Results and Discussion: Comparison of Theory and Experiments

4.1. Path Loss without Consideration of the Diffraction Effect

A specific environment was considered for the design of the algorithm. The study conducted research on a microcell. Thus, the establishment of a reasonable and general model is the premise for the prediction of the radio wave. An urban environment is characterized by the existence of numerous buildings. To simplify the model, the buildings are generally equivalent to a rectangular parallelepiped with smooth and flat surfaces. The flowers, trees, cars, and other factors are generally ignored, and the loss of the space caused by the scattering is not considered. Thus, the propagation environment of radio waves has been established. Radio waves mainly propagate in air and the directed, reflected, and diffracted rays from the walls, corners of the wall or the ground would occur. The measurement area was divided into two areas based on the propagation scenario: LOS and

NLOS. In this study, the equilateral triangle was split into different times, that is, there are 40,962, 163,842, 65,362, and 2,621,442 rays when it was split six, seven, eight, and nine times, respectively. The electric fields of the direct wave and the multiple reflection waves (up to five times) were calculated, and the path loss that changed with distance was obtained.

As shown in Figures 8 and 9, the path loss varied with the distance for the different number of rays in the LOS. The term 'meas' denotes measurements. The red line is the experimental data, and the blue and black lines are both theoretical calculations. The blue line is the sum-of-individual-ray-powers (SP) method, and the black line is the power-of-complex-sum (PS) method. The direct ray, first order reflection, second order reflection, third order reflection, fourth order reflection and fifth order reflection are considered in the theoretical calculation. The distance from the measured points to the transmitting antenna are used as values of the abscissas. When the receiver is away from the transmitter, the measured path loss increases as a function of distance in Figures 8 and 9. The PS and SP methods have minor differences from the measured data in the different number of rays, as shown in Figures 8 and 9. As listed in Table 2, the root mean square error (RMSE) of the SP method is less than the RMSE of the PS method, thus indicating that the SP method is better than the PS method in the LOS. When the number of rays is 40,962, the RMSE of the SP method is 4.5106, which is less than the corresponding RMSE values in the cases of other ray numbers. This implies that as the number of rays increased, the agreement between the theoretically calculated and the measured data improved.
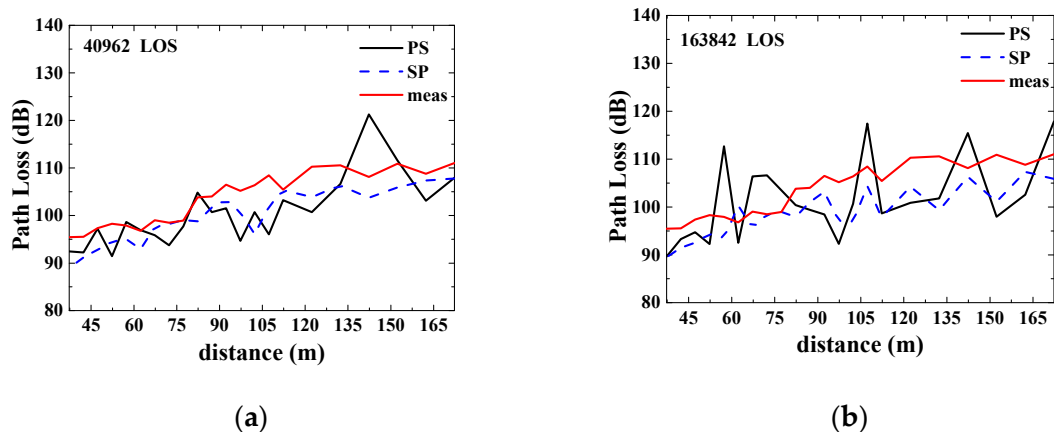
Figure 8. Path loss comparison of theoretical calculation with measured data for 40,962 and 163,842 rays in the LOS, respectively. (**a**) The number of rays is 40,962 (**b**) The number of rays is 163,842.
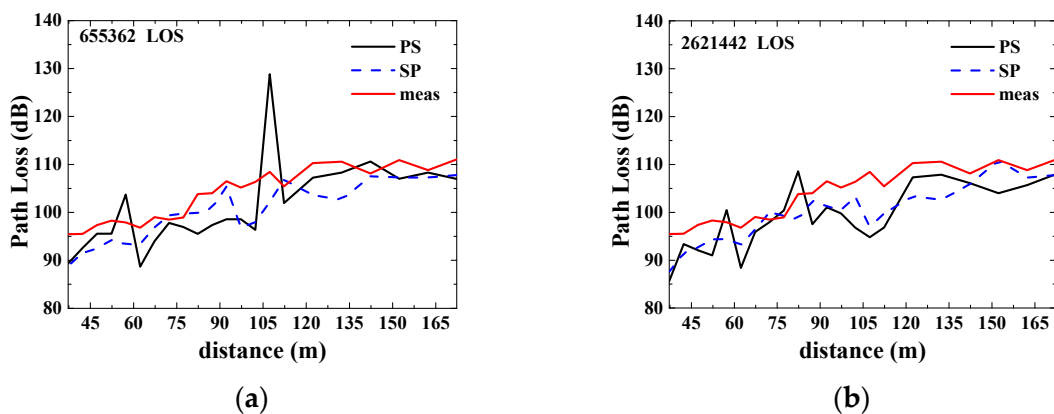
Figure 9. Path loss comparison of theoretical calculation with measured data for 655,362 and 2,621,442 rays in the LOS, respectively. (**a**) The number of rays is 655,362 (**b**) The number of rays is 2,621,442.

Table 2. The RMSE in the LOS.

The Number of the Ray	RMSE (SP)	RMSE (PS)
10,242	4.9240	6.3400
40,962	4.5106	5.8789
163,842	5.6778	7.8459
655,362	4.6707	6.6942
2,621,442	4.92323	6.1555

As shown in Figures 10 and 11, the path loss in the measured data increases as the distance between the transmitter and receiver in the NLOS environment increases and as the received power decreases. In theory, up to five orders of reflections are calculated. The theoretical calculation curves shown in Figures 10 and 11 are not continuous because the receiving antenna is in the NLOS environment relative to the transmitting antenna, and multiple reflections do not occur at the discontinuous receiving point. Therefore, this may be the received signal owing to diffraction. If the diffracted rays are not calculated, or if the effect of the diffracted rays is neglected, the received field strength becomes weaker and the path loss increases. It was found that when the rays were equal to 40,962, 163,842, 655,362, and 2,621,442, there were large differences between the theoretical calculation and experimental data, as shown in Figures 10 and 11. This shows that the diffraction has a significant influence on the electric field strength and the path loss in the NLOS environment.

(a)   (b)
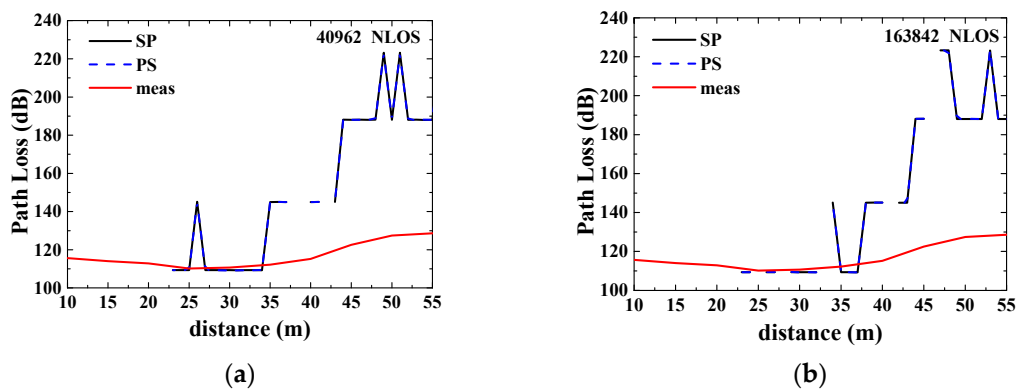
Figure 10. Path loss comparison of theoretical calculation with measured data for 40,962 and 163,482 rays in the NLOS, respectively. (**a**) The number of rays is 40,962 (**b**) The number of rays is 163,482.

(a)   (b)
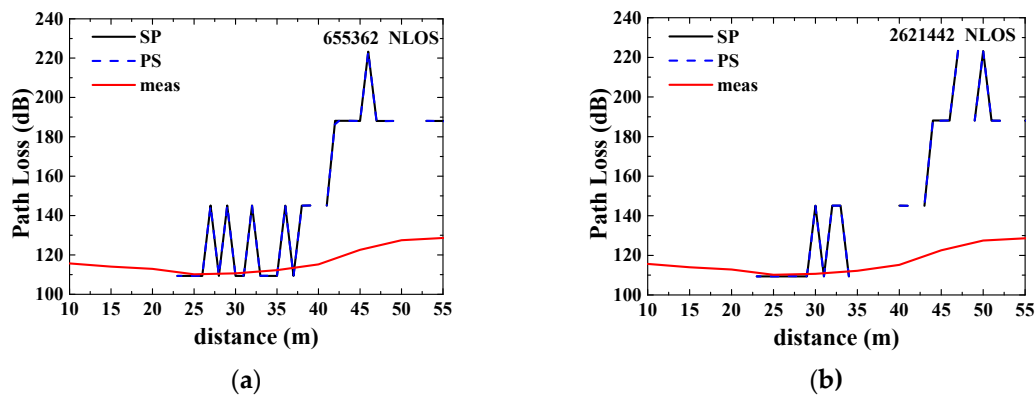
Figure 11. Path loss comparison of theoretical calculation with measured data for 655,362 and 2,621,442 rays in the NLOS, respectively. (**a**) The number of rays is 655,362 (**b**) The number of rays is 2,621,442.

4.2. Path Loss Considering the Diffraction Effect

According to the inference in Section 4.1, the diffraction phenomenon has a very important influence on the received signal in the microcellular environment. Therefore, the direct ray from the transmitter to the receiver, the specular reflection, over-rooftop diffraction, diffraction from a vertical edge, and the diffraction at the intersection of the wall and the ground are calculated and discussed in this section. The direct ray, first-order diffraction, reflection followed by diffraction, diffraction followed from reflection, and (up to five orders of) reflections were considered. The path loss at a certain distance was calculated in the study when the number of emitted rays was different in the LOS environment, as shown in Figures 12 and 13.
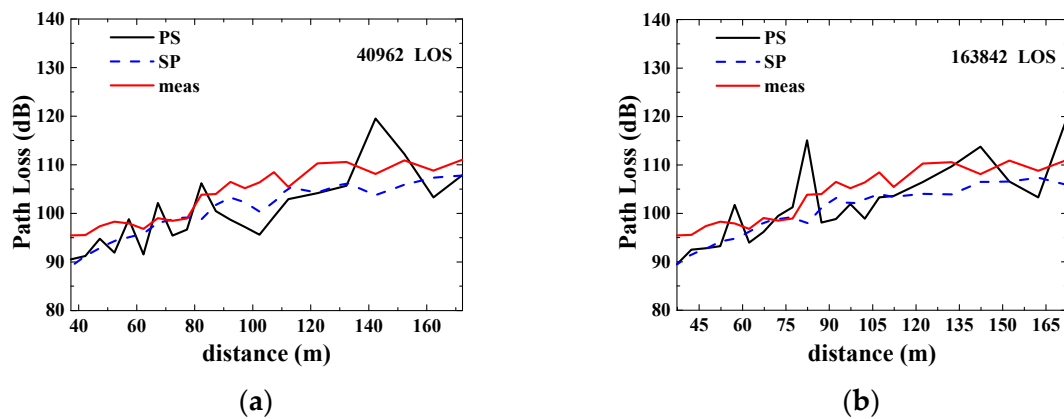
Figure 12. Path loss comparison of theoretical calculation with measured data for 40,962 and 163,482 rays in the LOS. (**a**) The number of rays is 40,962 (**b**) The number of rays is 163,482.
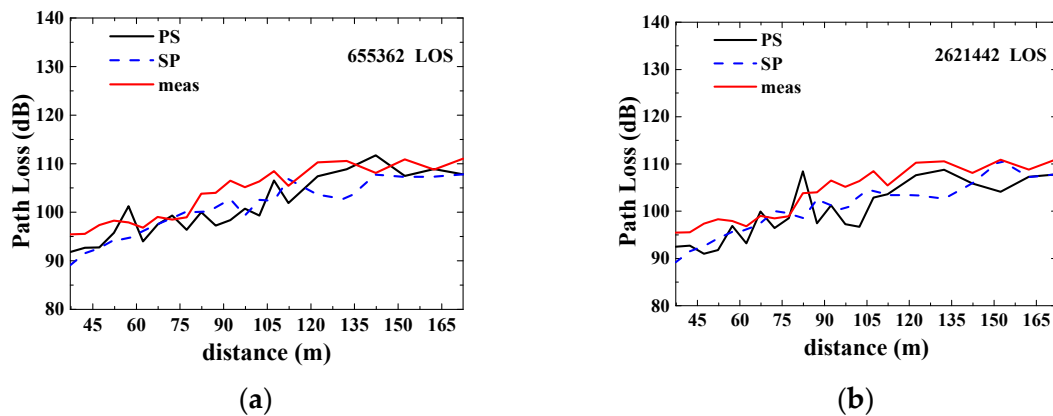
Figure 13. Path loss comparison of theoretical calculation with measured data for 655,362 and 2,621,442 rays in the LOS. (**a**) The number of rays is 655,362 (**b**) The number of rays is 2,621,442.

In Figures 12 and 13, the path loss varies as a function of distance between the transmitting and receiving antennas in the LOS environment. As the distance increases, the path loss will increase, and the received power will decrease. When 40,962 and 163,842 rays are used, the calculated results of the PS method do not fit well with the measured data. However, the calculated results of the PS method for 655,362 and 2,621,442 rays are generally in agreement with the measured data. The RMSE of the SP method is smaller than that of the PS method in general (Table 3). The RMSEs of the SP method with 40,962 rays and 163,842 rays are 3.9318 and 3.9212, respectively. The RMSEs of the SP method with 10,242, 655,362, and 2,621,442 rays are 4.1386, 4.1032, and 3.9704, respectively. Therefore, considering the calculation time and accuracy, the use of 40,962 rays is the best choice. The theoretical calculation and the measured data are in good agreement in general. When the

distance between the transmitting and receiving antennas is around 100 m, the SP method and the experimental data have a certain error, which is caused by the obstacles, such as by the surrounding cars, telegraph poles, and vegetation. However, the error is within the allowable range. The measured data are consistent with the theoretical calculations, thus indicating that the results obtained by the algorithm in this study are effective. The theoretical calculations of 40,962 rays are in good agreement with the measured data irrespective of whether diffraction was considered. The RMSE of the SP method was 4.5106 when diffraction was not considered. When diffraction was considered, the RMSE of the SP method was 3.9318. The two values were not very different, thus indicating that the diffraction effect was very weak in the LOS. However, the 3D ray launching method that considers the effect of diffraction can generally predict the electric field intensity of any field point near the communication base station. A 2D visualization of the propagation path from the transmitting (22.3, 64.9, 9) to the receiving (172.3, 71.3, 1.5) location is shown in Figure 14. There are numerous rays from the transmitting point to the receiving point, indicating multipath propagation.

Table 3. The RMSE in the LOS.

The Number of rays	RMSE (SP)	RMSE (PS)
10,242	4.1386	5.5011
40,962	3.9318	5.7427
163,842	3.9212	5.3059
655,362	4.1032	3.9049
2,621,442	3.9704	4.6499
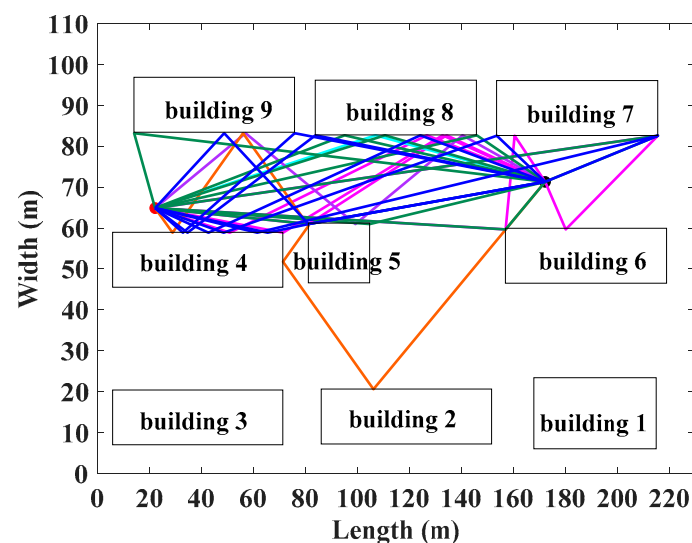
Figure 14. Visualization of the propagation path in a 2D surface at 172.3 m in the LOS.

In Figures 15 and 16, the path loss in a certain distance changes with the distance between the transmitting and the receiving antenna in the NLOS environment. It can be observed from these figures that when the distance is between 23 and 55 m, the difference between the theoretical calculation and the measured data is approximately 6 dB for 40,962, 163,842, and 655,362 rays. However, the difference between the theoretical calculation and the measured data is approximately 15 dB when the distance is between 10 and 23 m. This is attributed to the fact that when the diffraction is not considered, there are no multiple reflections from the transmitting to the receiving locations (between 10 and 23 m), and the path loss cannot be calculated. When the diffraction is considered, first-order diffraction, reflection followed by diffraction, and diffraction followed from reflection would occur from the transmitting to the receiving points. This shows that diffraction has a certain

effect in the NLOS case. The difference between the SP method and the measured data may be attributed to the fact that the surrounding fitness equipment and vegetation were ignored. The 3D ray launching method was in good agreement with the measured data as the distance varied between 23 and 55 m. The RMSE of the theoretical calculation is the smallest when the number of rays is 655,362, as shown in Table 4; that is, the RMSEs of the PS method are 8.5142 and 7.8922, respectively. This indicates that the theoretical calculation that considers the effect of diffraction is in a better agreement with the measured data compared with the 3D ray launching method that does not consider the effect of diffraction. This confirms the validity of the results obtained by the new ray launching method. A 2D visualization of the propagation path from the transmitting (2.9, 54.7, 9) to the receiving (60, 62.9, 1.5) antenna in the NLOS is shown in Figure 17. The figure shows that the number of rays in the NLOS is not as rich as the ones in the LOS. The 3D ray launching method that considered the effect of diffraction provided a theoretical basis for the urban radio wave transmission and the setting and optimization of the base station location.
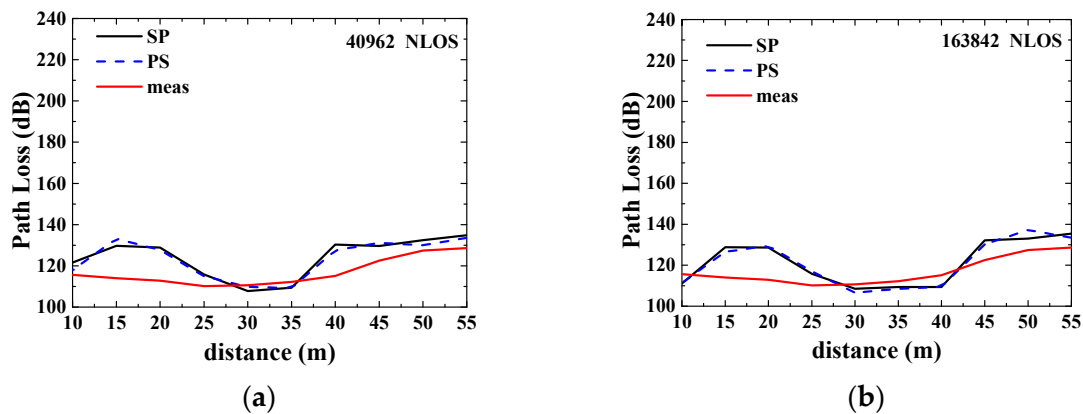
Figure 15. Path loss comparison of theoretical calculation with measured data for 40,962 and 163,842 rays in the NLOS. (**a**) The number of rays is 40,962 (**b**) The number of rays is 163,482.
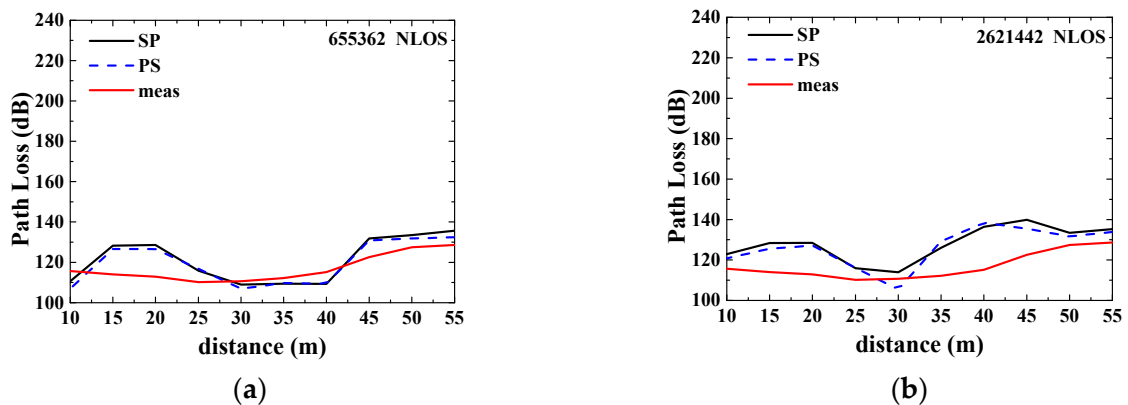
Figure 16. Path loss comparison of theoretical calculation with measured data for 655,362 and 2,621,442 rays in the NLOS. (**a**) The number of rays is 655,362 (**b**) The number of rays is 2,621,442.

Table 4. The RMSE in the NLOS.

The Number of the Ray	RMSE (SP)	RMSE (PS)
10,242	8.8742	8.9469
40,962	9.6515	9.4241
163,842	8.5696	8.6053
655,362	8.5142	7.8922
2,621,442	12.5075	12.1358
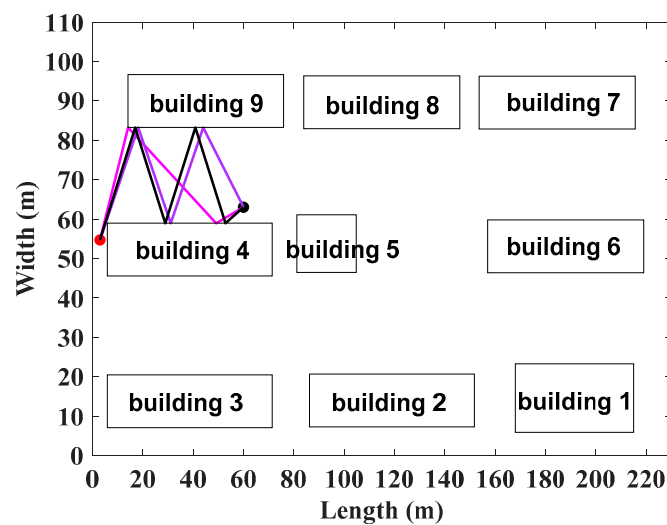
Figure 17. Visualization of the propagation path in a 2D surface at 60 m in the NLOS.

5. Conclusions

To improve the prediction accuracy of the signal in the millimeter wave in typical urban microcells, a channel measurement experiment at 39 GHz was conducted. Herein, a 3D ray launching method that considered the effect of diffraction was studied. The results showed that when diffraction was not considered in the 3D ray launching method in the outdoor microcell, the field strength of the receiving antenna cannot be calculated if the theoretical calculations appeared discontinuous in the NLOS propagation. Moreover, there were major differences between the theoretical calculations and experimental data in the cases of different number of rays in the NLOS propagation. This discrepancy may be caused by the diffraction effect. This means that the diffraction effect has a very important influence on the signal reception in the NLOS propagation. The diffraction effect was then considered in the 3D ray launching method. In the LOS propagation, the results showed that the RMSE of the 3D ray launching method that considered the diffraction effect was almost the same as the RMSE of the 3D ray launching method that did not consider the diffraction effect for 655,362 rays. This showed that the diffraction effect was very weak in the LOS propagation. In the NLOS propagation, the RMSEs of the PS and SP methods for 655,362 rays were 8.5142 and 7.8922, respectively. Moreover, the RMSE values obtained by considering the effect of diffraction were much smaller than those that did not consider the effect of diffraction in the NLOS propagation. The theoretical calculations that considered the effect of diffraction and the measurement data were in good agreement in general. Some deviations between the SP method and the measured data may be attributed to the influence of the surrounding environment. The above analysis showed that the diffraction effect should be considered in the 3D ray launching method in an outdoor microcell. Further studies on radio wave propagation in outdoor microcells will be of great significance for the selection and optimization of base station locations.

References

1. Saha, R.K. 3D spatial reuse of multi-millimeter-wave spectra by ultra-dense in-building small cells for spectral and energy efficiencies of future 6g mobile networks. *Energies* **2020**, *13*, 1748. [CrossRef]
2. Tavsanoglu, A.; Briso, C.; Carmena-Cabanillas, D.; Arancibia, R.B. Concepts of Hyperloop Wireless Communication at 1200 km/h: 5G, Wi-Fi, Propagation, Doppler and Handover. *Energies* **2021**, *14*, 983. [CrossRef]
3. Zhao, X.; Du, F.; Geng, S.; Fu, Z.; Wang, Z.; Zhang, Y.; Zhou, Z.; Zhang, L.; Yang, L. Playback of 5G and beyond measured MIMO channels by an ANN-based modeling and simulation framework. *IEEE J. Sel. Areas Commun.* **2020**, *38*, 1945–1954. [CrossRef]
4. Wu, Z.Z. *Mobile Communication Radio Wave Propagation*; Posts & TELECOM Press: Beijing, China, 2002.
5. Yuan, Z.W. *Theory and Method of Terminal Ray Tracing Positioning in Mobile Communication System*; Publishing House of Electronics Industry: Beijing, China, 2007.
6. ZTE. *5G Millimeter Wave Technology White Paper*; ZTE: Shenzhen, China, 2020.
7. Glassner, A.S. *An Introduction to Ray Tracing*; Academic Press Limited: London, UK, 1989.
8. Yun, Z.; Iskander, M.F. Ray tracing for radio propagation modeling: Principles and applications. *IEEE Access* **2015**, *3*, 1089–1100. [CrossRef]
9. Imai, T. A survey of efficient ray-tracing methods for mobile radio propagation analysis. *IEICE Trans. Commun.* **2016**, *E100–B*, 666–679.
10. He, D.; Ai, B.; Guan, K.; Wang, L.; Zhong, Z.; Kurner, T. The design and applications of high-performance ray-tracing simulation platform for 5G and beyond wireless communications: A tutorial. *IEEE Commun. Surv. Tutor.* **2018**, *21*, 10–27. [CrossRef]
11. Del Corte-Valiente, A.; Gómez-Pulido, J.M.; Gutiérrez-Blanco, O.; Castillo-Sequera, J.L. Localization Approach Based on Ray-Tracing Simulations and Fingerprinting Methods for Indoor–Outdoor Scenarios. *Energies* **2019**, *12*, 2943. [CrossRef]
12. Chen, Y.S.; Lai, F.P.; You, J.W. Analysis of antenna radiation characteristics using a hybrid ray tracing algorithm for indoor WiFi energy-harvesting rectennas. *IEEE Access* **2019**, *7*, 38833–38846. [CrossRef]
13. Seidel, S.Y.; Rappaport, T.S. Site-specific propagation prediction for wireless in-building personal communication system design. *IEEE Trans. Veh. Technol.* **1994**, *43*, 879–891. [CrossRef]
14. Durgin, G.; Patwari, N.; Rappaport, T.S. An advanced 3D ray launching method for wireless propagation prediction. *IEEE Veh. Technol. Conf. Phoeniz.* **1997**, *2*, 785.
15. Horikoshi, J.; Tanaka, K.; Morinaga, T. 1.2 GHz band wave propagation measurement in concrete building for indoor radio communications. *IEEE Trans. Veh. Technol.* **1986**, *35*, 146–152. [CrossRef]
16. Bultitude RJ, C.; Mahmoud SA Sullivan, W.A. A comparison of indoor radio propagation characteristics at 910 MHz and 1.75 GHz. *IEEE J. Sel. Areas Commun.* **1989**, *7*, 20–30. [CrossRef]
17. Arnold, H.W.; Murray, R.R.; Cox, D.C. 815 MHz radio attenuation measured within two commercial buildings. *IEEE Trans. Antennas Propagat.* **1989**, *37*, 1335–1339. [CrossRef]
18. Honcharenko, W.; Bertoni, H.L.; Dailing, J.L.; Qian, J.; Yee, H.D. Mechanisms governing UHF propagation on single floors in modern office buildings. *IEEE Trans. Veh. Technol.* **1992**, *41*, 496–504. [CrossRef]
19. Ji, Z.; Li, B.H.; Wang, H.X. Prediction of propagating from outdoor to indoor sites by using ray-tracing method. *J. China Inst. Commun.* **2001**, *22*, 114–119.
20. Schaubach, K.R.; Davis, N.J.; Rappaport, T.S. A Ray Tracing Method for Predicting Path Loss and Delay Spread in Microcellular Environments. In Proceedings of the Vehicular Technology Society 42nd VTS Conference-Frontiers of Technology, Denver, CO, USA, 10–13 May 1992; pp. 932–935.
21. He, W.; Zhang, M.; Bo, Y. A Fast Ray-Tracing Software Package for Field Distribution Predictions. In Proceedings of the 2016 IEEE International Workshop on Electromagnetics: Applications and Student Innovation Competition (iWEM), Nanjing, China, 16–18 May 2016; pp. 1–3.
22. Geok, T.K.; Hossain, F.; Chiat, A.T.W. A novel 3D ray launching technique for radio propagation prediction in indoor environments. *PLoS ONE* **2018**, *13*, e0201905. [CrossRef]
23. Hossain, F.; Geok, T.K.; Rahman, T.A.; Hindia, M.N.; Dimyati, K.; Ahmed, S.; Tso, C.P.; Abd Rahman, N.Z. An efficient 3-D ray tracing method: Prediction of indoor radio propagation at 28 GHz in 5G network. *Electronics* **2019**, *8*, 286. [CrossRef]
24. Erceg, V.; Rustako, A.J.; Roman, R.S. Diffraction around corners and its effects on the microcell coverage area in urban and suburban environments at 900 MHz, 2 GHz, and 4 GHz. *IEEE Trans. Veh. Technol.* **1994**, *43*, 762–766. [CrossRef]
25. Zhang, Y.; Wu, J.; Guo, L.; Zhao, Z.; Lin, L.; Xu, B.; Zhang, R. The quasi 3-D ray tracing model in microcellular environment. *Chin. J. Radio Sci.* **2012**, *27*, 954.
26. Zhang, M.G. *Tropospheric Scattering*; Publishing House of Electronics Industry: Beijing, China, 2004.
27. Tan, S.Y.; Tan, H.S. A theory for propagation path-loss characteristics in a city-street grid. *IEEE Trans. Electromagn. Compat.* **1995**, *37*, 333–342. [CrossRef]

28. Tan, S.Y.; Tan, H.S. UTD propagation model in an urban street scene for microcellular communications. *IEEE Trans. Electromagn. Compat.* **1993**, *35*, 423–428. [CrossRef]
29. Robert, G. Uniform Geometrical Theory of Diffraction for an Edge in a Perfectly Conducting Surface. *Proc. IEEE* **1974**, *62*, 116–130.
30. McNamara, D.A.; Malherbe, J.A.G.; Pistorius, C.W.I. *Introduction to the Uniform Geometrical Theory of Diffraction*; Artech House: Boston, MA, USA, 1990.
31. Wang, M.G. *The Geometric Diffraction Theory*; Xidian University Press: Xi'an, China, 1994.
32. Wu, J.F.; Cao, W.; Cheng, Y. A Two-Dimension Ray-Tracing Model for Microcellular Wave Propagation Prediction. *J. Nanjing Univ. Posts Telecommun.* **2001**, *21*, 45–51.